Elimination of remnant phases in low-temperature growth of wurtzite ScAlN by molecular-beam epitaxy

Brandon Dzuba, Trang Nguyen, Amrita Sen, et al.

View Online   Export Citation   CrossMark

Elimination of remnant phases in low-temperature growth of wurtzite ScAlN by molecular-beam epitaxy

Brandon Dzuba,[1,2] Trang Nguyen,[1] Amrita Sen,[3] Rosa E. Diaz,[2] Megha Dubey,[4] Mukesh Bachhav,[5] Janelle P. Wharry,[3] (ID) Michael J. Manfra,[1,2,3,6] (ID) and Oana Malis[1,2,a)] (ID)

AFFILIATIONS

[1]Department of Physics and Astronomy, Purdue University, West Lafayette, Indiana 47907, USA
[2]Birck Nanotechnology Center, West Lafayette, Indiana 47907, USA
[3]School of Materials Engineering, Purdue University, West Lafayette, Indiana 47907, USA
[4]Center for Advanced Energy Studies, Idaho Falls, Idaho 83401, USA
[5]Idaho National Laboratory, Materials and Fuel Complex, Scoville, Idaho 83415, USA
[6]School of Electrical and Computer Engineering, Purdue University, West Lafayette, Indiana 47907, USA

[a)]Author to whom correspondence should be addressed: omalis@purdue.edu

ABSTRACT

Growth of wurtzite $Sc_xAl_{1-x}N$ (x < 0.23) by plasma-assisted molecular-beam epitaxy on c-plane GaN at high temperatures significantly alters the extracted lattice constants of the material due to defects likely associated with remnant phases. In contrast, ScAlN grown below a composition-dependent threshold temperature exhibits uniform alloy distribution, reduced defect density, and atomic-step surface morphology. The c-plane lattice constant of this low-temperature ScAlN varies with composition as expected from previous theoretical calculations and can be used to reliably estimate alloy composition. Moreover, lattice-matched $Sc_{0.18}Al_{0.82}N$/GaN multi-quantum wells grown under these conditions display strong and narrow near-infrared intersubband absorption lines that confirm advantageous optical and electronic properties.

Published under an exclusive license by AIP Publishing. https://doi.org/10.1063/5.0118075

I. INTRODUCTION

Aluminum nitride (AlN), indium nitride (InN), and gallium nitride (GaN) have been major topics of interest in the materials and device communities in recent decades primarily due to the large range of bandgaps achievable using III-nitride alloys (0.64–6.2 eV). These materials have been used in the development of various electronic and optoelectronic devices such as light-emitting diodes, laser diodes, and high electron mobility transistors (HEMTs).[1] A persistent challenge throughout these III-nitride devices, however, is the large lattice mismatch between different alloys that can exceed 9% in InN/GaN heterostructures. The resulting strain leads to formation of defects that are detrimental to device performance. A potential solution to this problem is to utilize materials that are lattice-matched to the substrate, such as $In_{0.17}Al_{0.83}N$ layers on GaN. Unfortunately, $In_{0.17}Al_{0.83}N$ layers have been plagued with severe inhomogeneity issues[2–6] that

negatively impact optical characteristics.[7–10] Here, we investigate the structure and optical properties of the novel material wurtzite ScAlN, focusing on the Sc composition range around 18 at. % that is lattice-matched to c-plane GaN.

ScAlN has recently attracted attention due to its wide applicability in a variety of devices. ScAlN's large bandgap, spontaneous polarization,[7] and dielectric permittivity[8] can yield high two-dimensional electron gas densities, making it an attractive material for HEMTs and heterostructure field effect transistors (HFETs).[9–12] The enhanced electromechanical coupling of ScAlN relative to AlN[13] make the material ideal for electroacoustic resonators.[14–18] Furthermore, the significantly reduced etch rate of ScAlN compared to GaN and AlN make it suitable as an etch-stop layer for device fabrication.[19] Lastly, ScAlN is also emerging as a candidate for memory storage devices. ScAlN's slow shift of its internal lattice parameter with increasing scandium composition has been shown

to facilitate polarization switching[20] with polarization retention times exceeding 10^5 s.[21]

Many of the unique properties of ScAlN originate from its distinctive structural instability.[22–28] Unlike the commonly studied III-nitrides, $Sc_xAl_{1−x}N$ is stable in the wurtzite crystal phase only below x ≈ 0.55, and transitions to a rock-salt phase at higher Sc composition.[20,22,23] A metastable non-polar hexagonal, or h-BN-like phase, has also been proposed theoretically for ScN and ScAlN, but has not been confirmed experimentally.[24] Key material parameters of wurtzite ScAlN were first measured on polycrystalline sputter-deposited films[7,25–27] and calculated using density functional theory.[25–27] Structural parameters (lattice constants, stiffness coefficients, internal cell parameter, and bond angles) and other material parameters (dielectric constant, spontaneous polarization, and piezoelectric coefficients) are all believed to vary nonlinearly with composition,[26,28] but the scattering of reported experimental values may be due to differences in composition determination or mixed phases in the sputter-deposited material. Most notably, the change in bond angles and average bond lengths of relaxed wurtzite ScAlN with increasing Sc composition results in a relatively small and non-monotonic change in the c-plane lattice constant.[27] This makes the determination of alloy composition using the typical method of x-ray diffraction (XRD) problematic. Estimation of the scandium mole-fraction in ScAlN layers by XRD is further complicated by the reported growth-temperature dependence of the c-plane lattice constant.[29,30] Hardy et al. observed a monotonic increase in the XRD symmetric scan ω-2Θ peak angle with growth-temperature in $Sc_xAl_{1−x}N$ (x ≈ 0.18) layers grown on N-polar GaN substrates by molecular-beam epitaxy (MBE), despite little to no change in material composition. Under the circumstances, accurate estimation of the composition of ScAlN has been limited to time-consuming and expensive techniques such as Rutherford backscattering (RBS), energy dispersive x-ray spectroscopy (EDS), and x-ray photoelectron spectroscopy (XPS).

In this work, we seek to understand the link between growth temperature and crystalline structure in ScAlN, as well as to provide a framework for reliable compositional estimation of ScAlN by standard XRD techniques. We investigate wurtzite $Sc_xAl_{1−x}N$ growth by MBE on Ga-face (0001)-oriented GaN substrates across a range of compositions (x ≈ 0.11–0.23) and growth temperatures (450–760 °C). At high growth temperatures, for all compositions tested, we observe a dependence of the c-plane lattice constants in ScAlN on growth temperature, similar to that reported by Hardy et al. for $Sc_{0.18}Al_{0.82}N$.[29] Additionally, we find that the lattice constants of ScAlN grown at low temperature can be well explained by theory,[26] while those of high temperature ScAlN deviate significantly from theoretical predictions. Higher growth temperatures result in 3D growth, higher defect densities, higher surface roughness, and an inhomogeneous distribution of atoms within the material. These results may explain the deviation from theoretical lattice constants at higher temperatures. Lastly, we report for the first time near-infrared intersubband absorption with extremely narrow lines in lattice-matched $Sc_{0.18}Al_{0.82}N$/GaN multiple quantum wells (MQWs). This demonstrates the outstanding material and optical properties of low growth temperature MBE grown ScAlN, making it a promising material for future device applications.

II. EXPERIMENTAL

All nitride structures were grown by plasma-assisted MBE (PAMBE) on commercially available semi-insulating c-plane (0001)-oriented GaN on sapphire substrates with a reported treading dislocation density of $8 × 10^8$ cm$^{−2}$. The substrates were backside coated in 1 μm of tungsten silicide for improved thermal coupling and diced into quarters. Prior to loading into an ultrahigh vacuum (UHV) environment, the substrates were etched for 10 min in boiling HCl to remove any excess metals, sonicated in trichloroethylene, acetone, and methanol to remove any organic materials, and then rinsed with de-ionized water and dried with N_2 gas. The substrates were outgassed overnight (>12 h) at 550 °C in a UHV chamber attached to the MBE. The PAMBE system is equipped with conventional effusion cells for aluminum, indium, gallium, scandium, and silicon. A scandium source of 99.999% purity was used to reduce the reported negative effects of carbon, oxygen, and fluorine impurities.[31,32] A Veeco Unibulb radio-frequency (RF) plasma source is used to supply active nitrogen to the substrate. Prior to the active layer, a 150 nm GaN buffer layer is grown at 720 °C under gallium-rich conditions. This results in a GaN surface with pronounced atomically flat terraces and root-mean square (RMS) roughness <0.3 nm over 4 μm^2, as measured by atomic force microscopy (AFM) on control samples.

A series of 30–40 nm $Sc_xAl_{1−x}N$ films was grown across a range of compositions (0.11 < x < 0.23) and growth temperatures (450–760 °C) as measured by a pyrometer. All Sc-containing layers were grown within the nitrogen-rich regime, as metal-rich growth results in poor surface and structural quality[33] and the development of intermetallic phases on the surface.[34] The individual ScAlN films were grown with a III/V ratio between 0.6 and 0.8, while ScAlN used in the MQW structures used a III/V ratio of approximately 0.9. Plasma conditions of 305 W RF power with a 0.5 SCCM N_2 flow rate were used to generate an active nitrogen flux of ≈ $5.8 × 10^{14}$ atoms/cm^2 s, giving a nitrogen-limited GaN growth rate of approximately 7.9 nm/min. The MQW structures consisted of 50 repeats of $Sc_{0.18}Al_{0.82}N$/GaN followed by an additional ScAlN barrier to form the last quantum well (QW) and employed the gallium-rich growth method for the GaN layers. Excess gallium was incorporated into the structure by exposure to active nitrogen after each GaN layer. All MQWs were doped with silicon using a δ-doping scheme in which two sheets of silicon are placed inside the ScAlN barrier approximately 1 nm from each interface.

X-ray diffraction (XRD) reciprocal space mapping (RSM) and rocking curve measurements were made with a Panalytical Empyrean High-Resolution diffractometer, while XRD symmetric ω-2Θ scans were taken using a Panalytical X'Pert^3 MRD. Material thicknesses and MQW periods were determined either from thickness fringes in XRD symmetric ω-2Θ scans or by high-angle annular dark-field scanning transmission electron microscopy (HAADF-STEM) imaging. ScAlN material composition was determined by Rutherford backscattering (RBS) measurements conducted by EAG Laboratories, with an uncertainty in the scandium composition of ±1 at. %. The surface morphology of all samples was assessed using AFM.

MQW c-plane structures were investigated with HAADF-STEM. Acquisition was done with a double aberration-corrected Thermo Scientific Themis Z TEM/STEM at 300 kV acceleration voltage,

0.24 nA current, and 0.65 Å probe size. STEM samples were prepared using the focused ion beam (FIB) *in situ* liftout method on a Thermo Scientific Helios G4 UX Dual Beam FIB. Following the FIB process, the specimens were further thinned using a Fischione Nanomill Model 1040, working at 900 V, 120 μA, and ±10° tilt at low temperatures. Finally, each lamella was cleaned with a Fischione Ar Plasma Cleaner to remove any residue from the FIB and air.

Atom probe tomography (APT) was conducted to determine the chemical homogeneity of two $Sc_{0.18}Al_{0.82}N$ samples grown at different temperatures (550 and 720 °C). Specimens for APT were prepared by FIB milling. Due to the tendency of preferential evaporation of Ga during APT,[35–37] liftouts were made in cross section from the sample. All FIB work was done on the FEI (now Thermo Fisher Scientific) Quanta 3D FEG dual-beam FIB at the Center for Advanced Energy Studies (CAES), Idaho National Laboratory. Samples were analyzed using the CAMECA Local Electrode Atom Probe (LEAP) 4000X HR equipped with 355 nm UV laser, also at CAES. Specimens were analyzed under a wide range of LEAP running conditions selected to systematically investigate the influence of key parameters on the evaporation behavior and composition measurements, but ultimately the conditions of 0.1 pJ laser energy, 45 K base temperature, 200 kHz pulse rate, and 0.5% detection rate were chosen to minimize Ga preferential evaporation effects. A minimum of 2×10^6 ions were collected per needle to ensure statistical significance. APT data were processed and analyzed through CAMECA's Integrated Visualization and Analysis Software (IVAS version 3.8.4). Peaks in the APT mass spectra were ranged according to traditional mass ranging methods.[38]

Using a Thermo Scientific Nicolet 8700 spectrometer, direct Fourier transform infrared spectroscopy (FTIR) was utilized to measure intersubband absorption (ISBA) on all MQW samples.

The samples were polished into small pieces with 45° facets on both sides to let electromagnetic waves enter and be absorbed by the active region. The ISBA spectra were obtained by first normalizing the p- and s-polarized transmission spectra to the background, followed by calculating the ratio of the p- to s-polarized transmission spectra.

III. RESULTS AND DISCUSSION

Figure 1 summarizes the dependence of ScAlN lattice constants for the out-of-plane (0001) direction (c-axis) and in-plane (11$\bar{2}$0) direction (a-axis) on Sc composition and growth temperature (see the supplementary material for XRD RSM). Theoretical predictions for the wurtzite lattice constants are also included as curves in Fig. 1 for both ScAlN fully strained to GaN (red lines) and fully relaxed ScAlN (blue lines). These curves were obtained using the known values of the AlN lattice constants and the stiffness coefficients reported in Ambacher *et al.*[26] and Urban *et al.*[27] In agreement with previous reports,[29,30] we find $Sc_xAl_{1-x}N$ (x ≈ 0.18) grown at 720 °C to have an average c-plane lattice constant smaller than films grown at or below 550 °C. The effect is also clearly visible as a shift of the ScAlN XRD ω-2Θ peak toward larger angles (Fig. S4 in the supplementary material). This unusual behavior cannot be explained by a theory that predicts wurtzite $Sc_{0.18}Al_{0.82}N$ to be in-plane lattice-matched to GaN and, therefore, no elastic strain is expected at this composition. Residual strain due to thermal expansion mismatch also cannot justify the magnitude of this effect. Furthermore, we find the same correlation between c-plane lattice constant and growth temperature across a broad range of compositions (0.11 < x < 0.23) and growth temperatures (450–760 °C). Specifically, for all but the lowest investigated
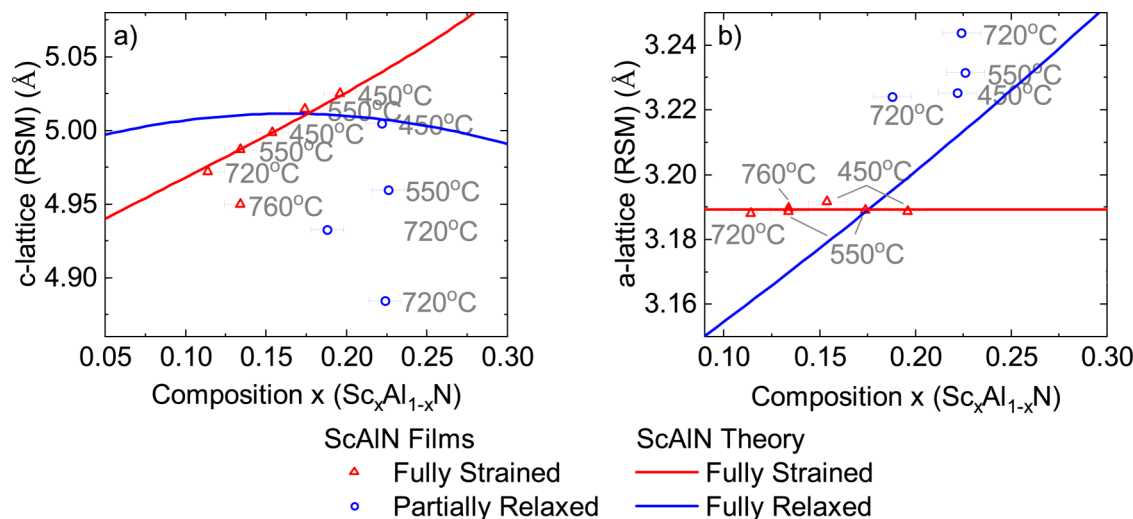

FIG. 1. (0001) c-plane lattice constants (a) and (11$\bar{2}$0) a-plane lattice constants (b) of ScAlN films determined from XRD RSM. The 30–40 nm thick ScAlN films have compositions near x ≈ 0.12, 0.18, 0.22, and were grown at temperatures of 450, 550, 720, or 760 °C, as indicated in the figure. The films were either fully coherent to the underlying GaN (red triangles) or exhibited some degree of relaxation (blue circles). Red and blue lines represent the theoretical lattice constants for ScAlN grown on GaN substrates, assuming either fully coherent or fully relaxed films, respectively. Error bars represent the error in film composition determined by RBS measurements.

composition, growth temperatures above 700 °C result in c-plane lattice constants significantly lower than theoretically predicted for either strained or relaxed ScAlN. For the largest Sc composition investigated (x ≈ 0.22), this c-plane lattice constant is even smaller than the value for pure AlN tensile-strained to GaN. We attribute the lower c-plane lattice constant to the existence of structural defects that are remnant of the non-polar hexagonal h-ScN phase. The signature of this h-BN-like phase is a c/a ratio smaller than the value for the wurtzite structure (1.63); a reduction of the c/a ratio has been previously observed in sputter-deposited ScAlN films.[20]

Figure 1 also indicates the strain state of the films extracted from RSM; coherently strained films use red symbols while partially relaxed films use blue symbols. For Sc composition above 20%, all films are partially relaxed regardless of growth temperature. At the highest growth temperatures, the measured c-plane lattice constant is significantly smaller than the expected value when the measured tensile strain state is considered. Moreover, the in-plane lattice constants of partially relaxed films are larger than expected for fully relaxed ScAlN [Fig. 1(b)]. This suggests that the deformation indicated by Fig. 1 is not solely due to changes in the strain state of the films, but must be caused by additional structural defects.

The available data suggest that below a composition-dependent growth temperature, the measured c-plane lattice constants for coherently strained ScAlN agree well with the values predicted by theory (red line).[26] This is true for films with scandium compositions x ≈ 0.12 and x ≈ 0.18 grown at and below 720 and 550 °C, respectively. Therefore, the composition of $Sc_xAl_{1-x}N$ films grown at low temperature can be reliably predicted for x ≤ 0.2 from XRD ω-2Θ scans. We note that film coherence to the substrate is a necessary, but not sufficient condition for the use of this composition determination method. For x > 0.2, the ScAlN films are partially relaxed, regardless of growth temperature, and composition needs to be determined using RBS, EDS, or XPS.

To further examine the effect of growth temperature on defect densities, XRD rocking curves were measured for the x ≈ 0.12 and

x ≈ 0.18 films (Fig. 2). We were unable to measure rocking curves for films with x > 0.2 due to the low intensity of the ScAlN peak coupled with its proximity to the intense GaN peak. For both compositions, the FWHM decreases with decreasing growth temperature. This trend confirms that growth at higher temperatures introduces defects into the material. The lowest growth-temperature samples have FWHM < 430 arc sec, similar to that reported by Wang et al.[30] AFM was also conducted on each film to assess surface morphology. AFM of all structures (see the supplementary material) grown at 550 °C presents atomic steps, indicating a step-flow growth mode. These films have an RMS surface roughness of <0.9 nm over $4\,\mu m^2$. Surface steps are not visible for any composition at growth temperatures above 550 °C, and further reduction below 550 °C results in less-defined atomic steps. The absence of atomic steps at higher growth temperatures reinforces the conclusion drawn from XRD data; lower growth temperatures result in higher-quality ScAlN.

Since compositional fluctuations can cause phase segregation, we utilized APT to assess the chemical variations within the ScAlN films. Two 100 nm $Sc_{0.18}Al_{0.82}N$ films capped with 250 nm GaN were grown at 550 and 720 °C for APT measurements. The frequency distribution analyses from APT tip reconstructions are presented in Fig. 3. The film grown at 550 °C has a uniform distribution of all atomic species, shown by the excellent fit between the experimental data and a binomial distribution [Figs. 3(a) and 3(b)]. The 720 °C film, however, shows an inhomogeneous distribution of aluminum atoms, with regions of lower Al atom number density [Figs. 3(c) and 3(d)]. In contrast, the Sc atom number density variation is smaller than that of Al atoms. Due to the non-monotonic dependence of c-plane lattice constants on Sc composition, higher Sc composition regions relative to the matrix could result in a lower average lattice constant, as seen in Fig. 1. High concentration ScAlN could also result in the formation of rock-salt regions,[20] but we found no evidence of this phase in high-resolution STEM.
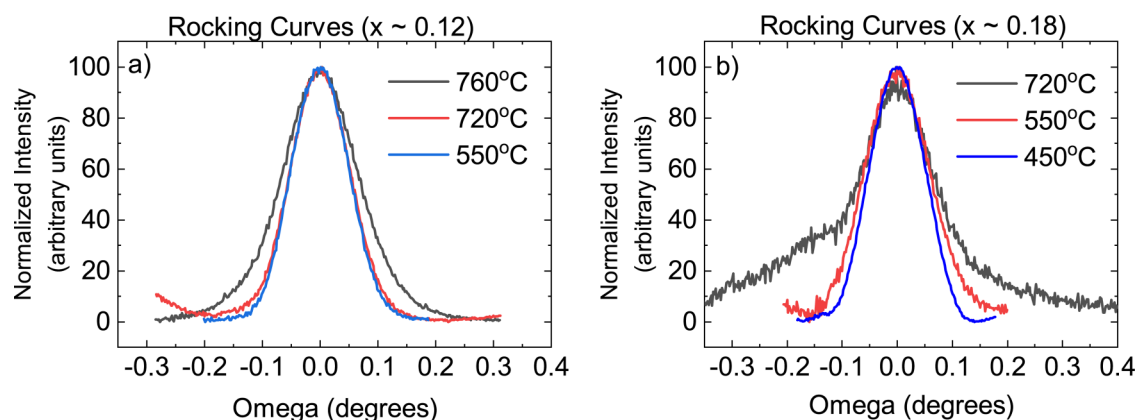

FIG. 2. XRD rocking curves of (0002) reflections for the ScAlN layers. (a) ScAlN layers with x ≈ 0.12, grown at 760, 720, and 550 °C, exhibit an FWHM of 0.155°, 0.118°, and 0.116°. (b) ScAlN layers with x ≈ 0.18 grown at 720 , 550, and 450 °C exhibit an FWHM of 0.167°, 0.136°, and 0.118°. Note that rocking curves were not measured for samples with x > 0.2 as the reduced intensity of the ScAlN XRD peak, coupled with the proximity to the intense GaN peak, made measurement of the peak impossible.
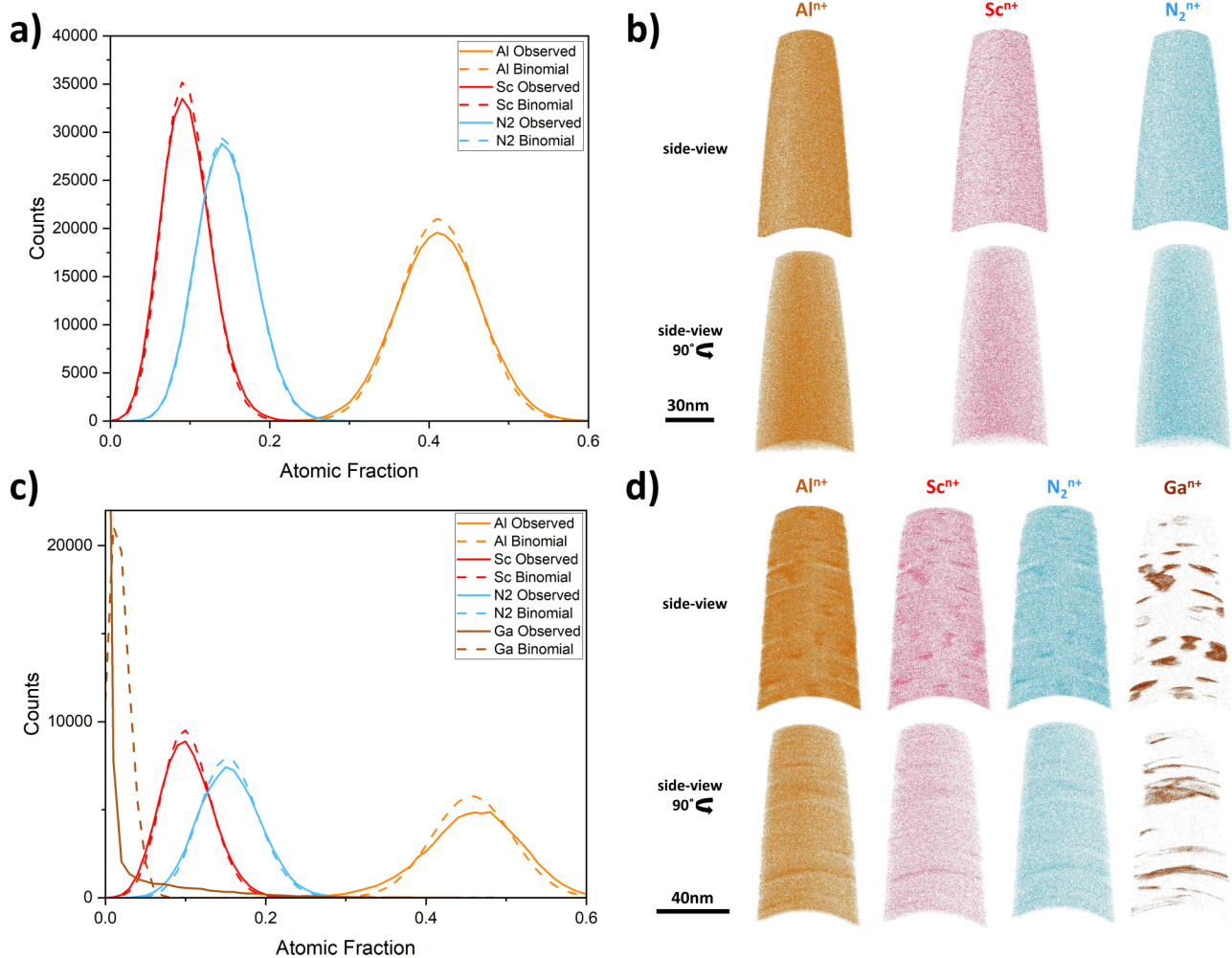
FIG. 3. APT frequency distribution of the ionic species and cross-sectional atomic density maps in $Sc_{0.18}Al_{0.82}N$ films grown at 550 °C [(a) and (b)] and 720 °C [(c) and (d)]. Deviation from binomial distribution indicates a non-uniform distribution of elements.

Surprisingly, gallium atoms were also detected in the $Sc_{0.18}Al_{0.82}N$ layer grown at 720 °C. APT compositional analysis shows that these Ga-containing regions may reach a composition as high as 20 at. % Ga (see the supplementary material). These nanometer-size regions were observed in all the 720 °C tips analyzed and are not a product of any gallium contamination from FIB preparation, as the gallium source used for FIB preparation is monoisotopic and would show a single peak (69 Da) in the mass spectra.[39] While a detailed analysis of these Ga-rich regions is outside the scope of this work, we suspect they are linked to defect generation at high growth temperatures that facilitates Ga diffusion into ScAlN during GaN cap deposition. The inclusion of even a small fraction of gallium could form ScGaN alloys that separate into zinc-blende phases even at low scandium compositions.[40] These Ga-containing defective phases likely alter the average lattice

constant of the material as we have seen in this report. Since the presence of these remnant defects is deleterious for the optical and electronic properties of ScAlN, it is preferable to suppress them altogether by focusing on low-temperature MBE growth. It is important to emphasize that these Ga-containing phases were not present in the films grown at 550 °C.

To assess the potential of low-temperature ScAlN for optical devices, we investigated near-infrared intersubband absorption in lattice-matched $Sc_{0.18}Al_{0.82}N$/GaN MQW heterostructures. HR-STEM of one of the $Sc_{0.18}Al_{0.72}N$/GaN heterostructures is shown in Fig. 4. HR-STEM reveals abrupt interfaces and a regular periodic structure. A series of MQWs was grown with a constant doping profile (silicon sheet density of 1.15×10^{13} cm^{-2}) but varying QW width (Fig. 5). QW widths of 8, 6, and 4 nm resulted in ISBA energies of 523, 567, and 611 meV with an FWHM of 52,

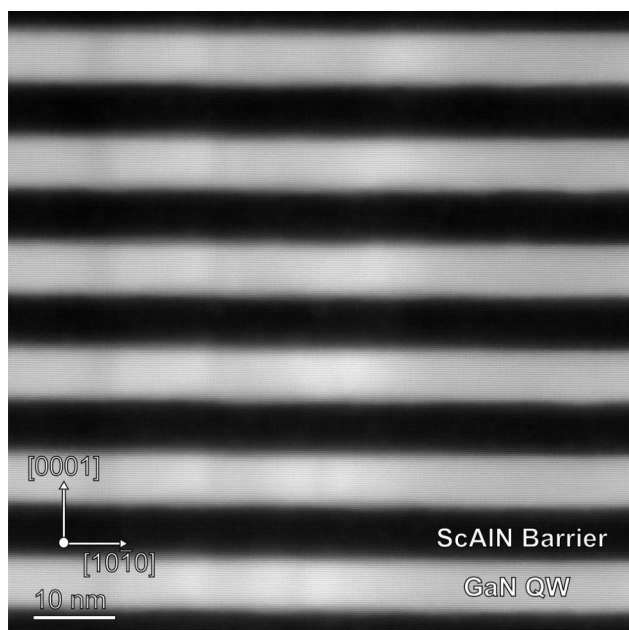**FIG. 4.** Dark-field HR-STEM of a $Sc_{0.18}Al_{0.82}N$/GaN (7×6 nm^2) MQW heterostructure with a silicon sheet density of 1.15×10^{13} cm^{-2}. Dark regions represent the ScAlN barriers, while light regions represent the GaN QWs.

50, and 45 meV, respectively. This trend of reduced ISBA energy with increasing QW width confirms that the absorption is due to intersubband transitions, while the narrow FWHM confirms the excellent structural quality. To the authors' knowledge, this is the first demonstration of near-IR ISBA in ScAlN/GaN MQW structures.
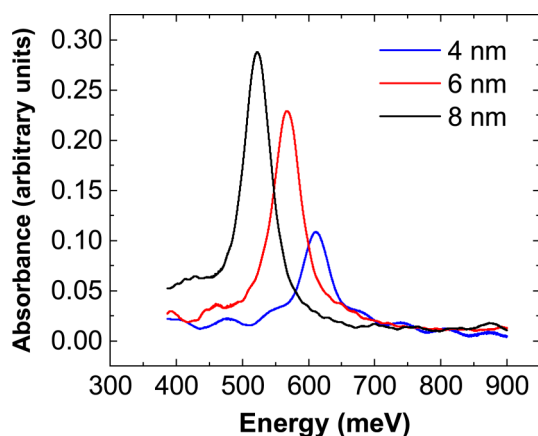

FIG. 5. Direct Fourier transform infrared (FTIR) absorption measurements of 50 repeat $Sc_{0.18}Al_{0.82}N$/GaN MQWs (QW width 4, 6, and 8 nm) with a barrier width of 7 nm and a silicon sheet density of 1.15×10^{13} cm^{-2}.

IV. CONCLUSION

Wurtzite $Sc_xAl_{1-x}N$ ($x < 0.23$) with outstanding structural and optical properties was grown by standard PAMBE at temperatures lower than typically used for Al(Ga)N. We investigated a series of 30–40 nm thick ScAlN films grown on Ga-face (0001)-oriented GaN/sapphire substrates across a range of scandium compositions ($0.11 < x < 0.23$) and growth temperatures (450–760 °C). The lattice parameters of these films were extracted from XRD RSM and compared to theoretical predictions. For all except the lowest composition studied ($x = 0.11$), we find a correlation between the c-plane lattice constant and growth temperature. The c-plane lattice constant of films grown at high temperatures (i.e., typically above 700 °C) is smaller than the value predicted by theory and smaller than the lattice constant of films grown at low temperatures. RSM measurements verify that this variation of c-plane lattice constant is not due to elastic relaxation in the material. XRD rocking curves indicate that higher growth temperatures lead to the generation of additional defects. In contrast, for low growth temperatures, the c-plane lattice constants agree with theoretical predictions, suggesting that XRD techniques can be used to reliably estimate the composition of coherently strained films with $x < 0.2$. This also eliminates the need to perform a more sophisticated composition analysis. Moreover, the surface morphology also improves at lower growth temperatures, with pronounced atomic steps visible for all films grown at 550 °C. APT analysis of two $Sc_{0.18}Al_{0.82}N$ films grown at different temperatures shows a drastic increase in material homogeneity at 550 °C, and severe chemical inhomogeneity present in the sample grown at 720 °C. We conclude that high temperature growth leads to defect generation in MBE grown ScAlN that may cause the observed temperature dependence of the c-plane lattice parameter.

Using the optimal growth conditions for $Sc_{0.18}Al_{0.82}N$, a series of silicon-doped lattice-matched ScAlN/GaN MQWs was grown and near-infrared ISBA was measured to probe the existence of well-defined confined electronic states. Strong and narrow near-infrared absorption lines are observed for the first time in Sc-containing nitride heterostructures. These optical results demonstrate the high quality of low-temperature ScAlN and reinforce its relevance for a wide range of devices.

SUPPLEMENTARY MATERIAL

See the supplementary material for RSM scans and AFM images of the 30–40 nm ScAlN films. Supplementary material also includes XRD symmetric ω-2Θ scans for the $x \approx 0.18$ ScAlN films and APT composition profiling of the 720 °C, $x \approx 0.18$, 100 nm thick film.

ACKNOWLEDGMENTS

at the Electron Microscopy Facility at the Birck Nanotechnology Center, Purdue University. APT characterization was performed at the Center for Advanced Energy Studies, with support from the U.S. Department of Energy, Office of Nuclear Energy, through Nuclear Science User Facilities (NSUF) under Award No. 20-2946.

AUTHOR DECLARATIONS
Conflict of Interest

Author Contributions

Brandon Dzuba: Investigation (equal); Writing – original draft (equal). **Trang Nguyen:** Investigation (equal). **Amrita Sen:** Investigation (equal); Writing – original draft (equal). **Rosa E. Diaz:** Investigation (equal). **Megha Dubey:** Investigation (equal). **Mukesh Bachhav:** Investigation (equal). **Janelle P. Wharry:** Investigation (equal); Supervision (equal); Writing – original draft (equal). **Michael J. Manfra:** Investigation (equal); Supervision (equal); Writing – original draft (equal). **Oana Malis:** Conceptualization (equal); Funding acquisition (equal); Writing – original draft (equal).

DATA AVAILABILITY

The data that support the findings of this study are available within the article.

REFERENCES

[1] O. Ambacher, J. Phys. D: Appl. Phys. **31**, 2653 (1998).
[2] S. Choi, F. Wu, R. Shivaraman, E. C. Young, and J. S. Speck, Appl. Phys. Lett. **100**, 232102 (2012).
[3] S. Dasgupta, S. Choi, F. Wu, J. S. Speck, and U. K. Mishra, Appl. Phys. Express **4**, 045502 (2011).
[4] W. Kong, W. Y. Jiao, J. C. Li, K. Collar, J. H. Leach, J. Fournelle, T. H. Kim, and A. S. Brown, J. Electron. Mater. **45**, 654 (2016).
[5] L. Zhou, D. J. Smith, M. R. McCartney, D. S. Katzer, and D. F. Storm, Appl. Phys. Lett. **90**, 081917 (2007).
[6] S.-L. Sahonta, G. P. Dimitrakopulos, T. Kehagias, J. Kioseoglou, A. Adikimenakis, E. Iliopoulos, A. Georgakilas, H. Kirmse, W. Neumann, and P. Komninou, Appl. Phys. Lett. **95**, 021913 (2009).
[7] M. A. Caro, S. Zhang, T. Riekkinen, M. Ylilammi, M. A. Moram, O. Lopez-Acevedo, J. Molarius, and T. Laurila, J. Phys.: Condens. Matter **27**, 245901 (2015).
[8] J. Casamento, H. Lee, T. Maeda, V. Gund, K. Nomoto, L. van Deurzen, W. Turner, P. Fay, S. Mu, C. G. Van de Walle, A. Lal, H. (Grace) Xing, and D. Jena, Appl. Phys. Lett. **120**, 152901 (2022).
[9] A. J. Green, J. K. Gillespie, R. C. Fitch, D. E. Walker, M. Lindquist, A. Crespo, D. Brooks, E. Beam, A. Xie, V. Kumar, J. Jimenez, C. Lee, Y. Cao, K. D. Chabak, and G. H. Jessen, IEEE Electron Device Lett. **40**, 1056 (2019).
[10] P. Wang, D. Wang, B. Wang, S. Mohanty, S. Diez, Y. Wu, Y. Sun, E. Ahmadi, and Z. Mi, Appl. Phys. Lett. **119**, 082101 (2021).
[11] A. J. Green, N. Moser, N. C. Miller, K. J. Liddy, M. Lindquist, M. Elliot, J. K. Gillespie, R. C. Fitch, R. Gilbert, D. E. Walker, E. Werner, A. Crespo, E. Beam, A. Xie, C. Lee, Y. Cao, and K. D. Chabak, IEEE Electron Device Lett. **41**, 1181 (2020).
[12] T. E. Kazior, E. M. Chumbes, B. Schultz, J. Logan, D. J. Meyer, and M. T. Hardy, in *2019 IEEE MTT-S International Microwave Symposium (IMS)* (IEEE, 2019), pp. 1136–1139.
[13] G. Wingqvist, F. Tasnádi, A. Zukauskaite, J. Birch, H. Arwin, and L. Hultman, Appl. Phys. Lett. **97**, 112902 (2010).
[14] W. Wang, P. M. Mayrhofer, X. He, M. Gillinger, Z. Ye, X. Wang, A. Bittner, U. Schmid, and J. K. Luo, Appl. Phys. Lett. **105**, 133502 (2014).
[15] W. B. Wang, Y. Q. Fu, J. J. Chen, W. P. Xuan, J. K. Chen, X. Z. Wang, P. Mayrhofer, P. F. Duan, A. Bittner, U. Schmid, and J. K. Luo, J. Micromech. Microeng. **26**, 075006 (2016).
[16] R. Dargis, A. Clark, A. Ansari, Z. Hao, M. Park, D. Kim, R. Yanka, R. Hammond, M. Debnath, and R. Pelzel, Phys. Status Solidi A **217**, 1900813 (2020).
[17] A. Ding, L. Kirste, Y. Lu, R. Driad, N. Kurz, V. Lebedev, T. Christoph, N. M. Feil, R. Lozar, T. Metzger, O. Ambacher, and A. Žukauskaitė, Appl. Phys. Lett. **116**, 101903 (2020).
[18] V. J. Gokhale, B. P. Downey, M. T. Hardy, E. N. Jin, J. A. Roussos, and D. J. Meyer, in *2020 IEEE 33rd International Conference on Micro Electro Mechanical Systems (MEMS)* (IEEE, Vancouver, BC, 2020), pp. 1262–1265.
[19] M. T. Hardy, B. P. Downey, D. J. Meyer, N. Nepal, D. F. Storm, and D. S. Katzer, IEEE Trans. Semicond. Manuf. **30**, 475 (2017).
[20] S. Zhang, D. Holec, W. Y. Fu, C. J. Humphreys, and M. A. Moram, J. Appl. Phys. **114**, 133510 (2013).
[21] P. Wang, D. Wang, N. M. Vu, T. Chiang, J. T. Heron, and Z. Mi, Appl. Phys. Lett. **118**, 223504 (2021).
[22] S. Barth, H. Bartzsch, D. Gloess, P. Frach, T. Modes, O. Zywitzki, G. Suchaneck, and G. Gerlach, Proc. SPIE **9517**, 951704 (2015).
[23] R. Deng, S. R. Evans, and D. Gall, Appl. Phys. Lett. **102**, 112103 (2013).
[24] N. Farrer and L. Bellaiche, Phys. Rev. B **66**, 201203 (2002).
[25] S. Zhang, W. Y. Fu, D. Holec, C. J. Humphreys, and M. A. Moram, J. Appl. Phys. **114**, 243516 (2013).
[26] O. Ambacher, B. Christian, N. Feil, D. F. Urban, C. Elsässer, M. Prescher, and L. Kirste, J. Appl. Phys. **130**, 045102 (2021).
[27] D. F. Urban, O. Ambacher, and C. Elsässer, Phys. Rev. B **103**, 115204 (2021).
[28] F. Tasnádi, B. Alling, C. Höglund, G. Wingqvist, J. Birch, L. Hultman, and I. A. Abrikosov, Phys. Rev. Lett. **104**, 137601 (2010).
[29] M. T. Hardy, B. P. Downey, N. Nepal, D. F. Storm, D. S. Katzer, and D. J. Meyer, Appl. Phys. Lett. **110**, 162104 (2017).
[30] P. Wang, D. A. Laleyan, A. Pandey, Y. Sun, and Z. Mi, Appl. Phys. Lett. **116**, 151903 (2020).
[31] J. Casamento, H. Lee, C. S. Chang, M. F. Besser, T. Maeda, D. A. Muller, H. (Grace) Xing, and D. Jena, APL Mater. **9**, 091106 (2021).
[32] J. Casamento, H. G. Xing, and D. Jena, Phys. Status Solidi B **257**, 1900612 (2020).
[33] M. T. Hardy, E. N. Jin, N. Nepal, D. S. Katzer, B. P. Downey, V. J. Gokhale, D. F. Storm, and D. J. Meyer, Appl. Phys. Express **13**, 065509 (2020).
[34] K. Frei, R. Trejo-Hernández, S. Schütt, L. Kirste, M. Prescher, R. Aidam, S. Müller, P. Waltereit, O. Ambacher, and M. Fiederle, Jpn. J. Appl. Phys. **58**, SC1045 (2019).
[35] J. R. Riley, R. A. Bernal, Q. Li, H. D. Espinosa, G. T. Wang, and L. J. Lauhon, ACS Nano **6**, 3898 (2012).
[36] D. R. Diercks, B. P. Gorman, R. Kirchhofer, N. Sanford, K. Bertness, and M. Brubaker, J. Appl. Phys. **114**, 184903 (2013).
[37] E. D. Russo, I. Blum, J. Houard, M. Gilbert, G. Da Costa, D. Blavette, and L. Rigutti, Ultramicroscopy **187**, 126 (2018).
[38] D. J. Larson, T. J. Prosa, R. M. Ulfig, B. P. Geiser, and T. F. Kelly, *Local Electrode Atom Probe Tomography* (Springer, New York, 2013).
[39] F. Tang, M. P. Moody, T. L. Martin, P. A. J. Bagot, M. J. Kappers, and R. A. Oliver, Microsc. Microanal. **21**, 544 (2015).
[40] S. M. Knoll, S. K. Rhode, S. Zhang, T. B. Joyce, and M. A. Moram, Appl. Phys. Lett. **104**, 101906 (2014).